ELSEVIER

Journal of Crystal Growth 216 (2000) 483–494

JOURNAL OF CRYSTAL GROWTH

www.elsevier.nl/locate/jcrysgro

Microsegregation in Peltier interface demarcation

Y. Dabo[a], H. Nguyen Thi[a,*], S.R. Coriell[b], G.B. McFadden[b], Q. Li[a,1], B. Billia[a]

[a]*L2MP, Université d'Aix–Marseille III et CNRS, Faculté des Sciences de Saint-Jérôme, Case 151, F-13397 Marseille Cedex 20, France*
[b]*National Institute of Standards and Technology, Gaithersburg, MD 20899, USA*

Received 11 February 2000; accepted 3 April 2000
Communicated by D.T.J. Hurle

Abstract

Experimental results on solute microsegregation induced by Peltier interface demarcation (PID) technique during directional solidification of Bi–1 wt% Sb alloys are presented. These data are compared with the results of numerical simulation and the theory of PID is revisited. It is shown that the Peltier coefficient previously determined using Peltier pulsing has been underestimated. The quantity of interface cooling absorbed by limited Bi-growth kinetics is comparable to that covered by solute depletion, and can even be dominant for very short pulses, so that the commonly made assumption of local equilibrium at the solid–liquid interface (i.e. usual hypothesis of constant interface temperature during pulse marking for pure systems) should be abandoned and the right dependence of interface temperature on solidification velocity be included in the model. Finally, two conditions to select systems capable of efficient marking by PID microsegregation are deduced and the effects of applied current in the first instants of electric pulse clarified.

Keywords: Alloy solidification; Bismuth–antimony; Peltier effect; Microsegregation

1. Introduction

During binary alloy solidification from the melt, the Mullins–Sekerka instability [1], drives the breakdown of the planar solid–liquid (S–L) interface and leads to the formation of nonplanar patterns (cells, dendrites). Several recent theoretical works [2–5] are focused on the initial transient of growth, that follows the application of the pulling rate, and its role in the building of cellular, or dendritic, arrays. In order to check the predictions of these theoretical analyses, it is crucial to explore the complete history of the pattern, from the early stages of the experiment to the asymptotic state.

The observation of the S–L interface is a major problem in the study of crystal growth from the melt. Only transparent systems allow easy in situ observation under an optical microscope. For metallic alloys and other opaque systems, the Peltier interface demarcation technique (PID) is appealing as the rapid freezing of the solidification microstructure by the usual quenching method hardly provides information on the evolution of the S–L interface morphology. PID takes advantage of the thermoelectric effects induced by a short-current

* Corresponding author. Tel.: +33-491-288673; fax: +33-491-288775.
E-mail address: nthenri@matop.u-3mrs.fr (H. Nguyen Thi).
[1] Present address: University of Iowa, USA.

0022-0248/00/$ - see front matter
PII: S0022-0248(00)00458-9

pulse of high intensity passing through the directionally solidifying sample. Indeed, such a pulse creates a perturbation of the S–L interface temperature and velocity that is accompanied by a variation of solute concentration. A series of electric pulses thus results in a series of solute-concentration variations which, after being revealed by proper metallography, delineate the instantaneous interface shape at successive times during growth and enables one to follow the time evolution of the S–L interface.

Several experimental and theoretical studies of the effects of an electric current on solidification or crystal growth have been carried out over the years, starting from the early works of Pfann and coworkers [6,7], who argued that the Peltier coefficient of the crystal–melt interface can be determined from the change in growth rate following the initiation of thermoelectric cooling by reversing the DC current. Since, several groups have contributed to the improvement of the technique and/or the deepening of the modelling [8–13]. It follows that PID is capable of providing critical information on time-dependent behaviours occurring in crystal growth [14–16]. Besides, PID was proved adequate to precisely investigate the birth and development of morphological instability [17,18], whose analysis was extended to include the influence of an electric current [19–21]. Yet, PID has up to now not been extensively used to study microstructure formation in solidification. Beyond the fact that metallography is very time consuming, the major reasons are probably that (i) detailed experimental knowledge of the fundamental aspects of PID is still lacking and (ii) marking by solute microsegregation has appeared to be poor for metallic systems, that gives no clear outline of the growth front on pictures. Indeed, it follows from practice that PID is sharp only in the case of materials with high thermoelectric coefficients such as Ge–Ga and Bi-based alloys or doped InSb.

Actually, the change of S–L interface temperature resulting from PID consists of two parts as for *any* material, and in particular for nonmetallic materials for which attachment kinetics is rather sluggish, the Gibbs–Thomson equation must include a kinetic term ΔT_k that measures the departure from thermodynamic equilibrium (see, e.g. Ref. [22]). Then, the boundary condition for temperature at a flat S–L interface reads

$$T_\phi = T_M + mC_L - \Delta T_k, \tag{1}$$

where T_ϕ is the interface temperature, T_M the pure-material melting temperature, m the liquidus slope and C_L the solute concentration in the liquid at the interface. Eq. (1) is in strong contrast with most papers on PID, in which the authors assume local thermodynamic equilibrium at the solidification front (i.e. constant interface temperature for a pure material) and only consider the heat-flux balance at the S–L interface.

Assuming that boundary condition (1) remains valid during the electric pulse (e.g. no solute trapping), one is able to deduce at any time t during the pulse the variation of interface temperature from its unperturbed value

$$(T_\phi)_t - (T_\phi)_0 = m[(C_L)_t - (C_L)_0] - [(\Delta T_k)_t - (\Delta T_k)_0], \tag{2a}$$

where the subscript 0 refers to the switching on of the electrical current, or, as it is the solute microsegration *in the solid* that is critical in the technique:

$$(T_\phi)_t - (T_\phi)_0 = n[(C_S)_t - (C_S)_0] - [(\Delta T_k)_t - (\Delta T_k)_0], \tag{2b}$$

where n ($= m/k$, with k the solute segregation coefficient) is the solidus slope and C_S the solute concentration in the solid.

The first term on the r.h.s. of Eqs. 2a and 2b is the basic ingredient of interface demarcation during directional solidification of a *binary alloy*, namely a "sharp" variation in composition at the solidification front during the electric pulse, sharp meaning sufficient for obtaining precise delineation of the shape of the S–L interface by metallography. The second term expresses the kinetic effect, which would be the only part remaining for a *pure material*.

In this paper, our main purpose is to analyse by a combined experimental and theoretical approach the solute contribution during directional solidification of a binary Bi–1 wt% Sb alloy. Then, the fundamental physical mechanisms ruling PID are

identified and the conditions that an alloy system should satisfy for optimum application of PID clarified.

2. Microsegregation induced by current pulses

2.1. Experimental procedure

For the present investigation, we use the directional solidification apparatus with a PID device which was previously described in detail [12]. Two heaters and a cooling zone can be translated over the fixed sample. The sample is held vertically in a quartz tube (8.5 mm inner diameter, 49 cm long) and solidification proceeds from bottom to top, in an Ar–5% H_2 ambient at a slight over-pressure of 1 mmHg. The electronic control system for the PID experiments is shown schematically in Fig. 1a. The electric contact at the top of the sample is obtained by using a 2 mm diameter molybdenum wire immersed in the melt while the other electric contact is the seed holder. For this study, the current density $I = 60\,A/cm^2$ and the current direction is from solid to liquid, such that Peltier cooling results and the solidification front moves faster during the pulse (for a description of the thermoelectric effects during a DC-electric pulse, the reader is referred to Refs. [10,12]).

In the experiments, a polycrystalline bismuth–1 wt% antimony sample, whose relevant material parameters are given in Table 1, is solidified in a liquid temperature gradient of 50 K/cm at different pulling velocities. From back-reflection Laue diagrams, the growth direction after some time of solidification is found to be nearly parallel to the bisectrix axis $[1\,1\,\bar{2}]$, which is long known to be the preferred growth direction of pure Bi [23] due to the marked anisotropy in thermal conductivity. This result is normal for Bi–Sb alloys, especially when the concentration is < 10 wt% Sb [24].

After solidification, the observation of the S–L interface morphology is made on longitudinal sections. After mechanical polishing, each section is etched to reveal the interface demarcation striations which are finally observed using Nomarski interference–contrast microscopy as shown in Fig. 1b.

Axial macrosegregation is obtained by chemical analysis of thin slices cut all along the sample while electron microprobe is used for radial macrosegregation. As shown in Fig. 2a, except for initial and

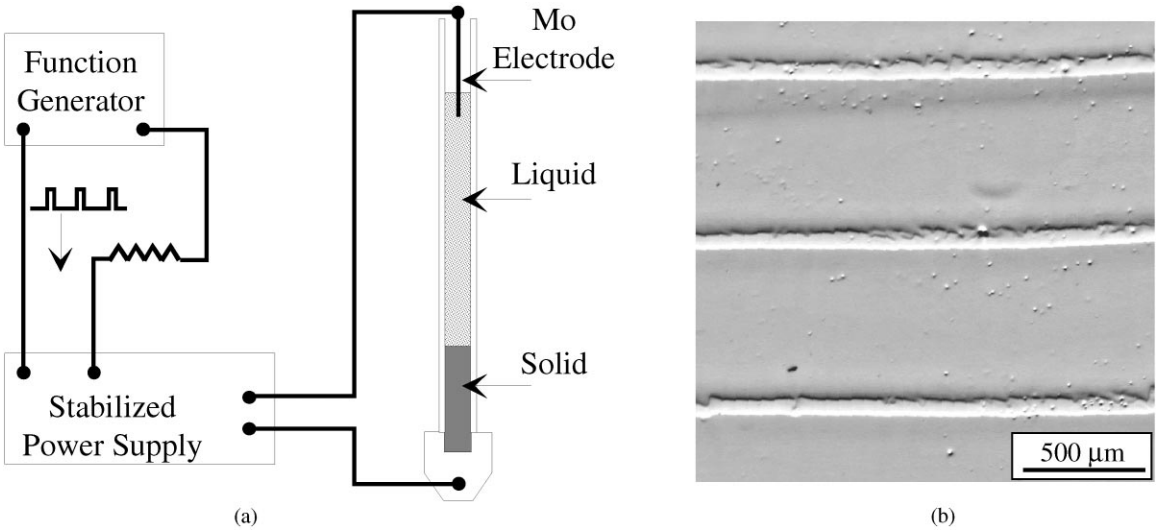

Fig. 1. (a) Control system for Peltier interface demarcation. (b) Optical micrograph of a longitudinal section showing the typical morphology of pulse marking striations. $V = 4.17\,\mu m/s$ and $\Delta t = 4\,s$.

Table 1
Thermophysical properties of bismuth–antimony alloys

Property	Symbol	Value	Units	Ref.
Segregation coefficient	k	1.97		
Liquidus slope	m	6.8	K/wt%	
Diffusion coefficient of Sb in liquid Bi	D_L	2.5×10^{-5}	cm^2/s	[25]
Melting point of pure Bi	T_M	544.4	K	
Heat of fusion	L	530	J/cm^3	
Liquid thermal conductivity	k_L	0.124	J/cm K s	[10]
Solid thermal conductivity	k_S	0.065	J/cm K s	[10]
Liquid specific heat	C_{pL}	1.46	J/cm^3 K	[10]
Solid specific heat	C_{pS}	1.46	J/cm^3 K	[10]
Liquid electrical conductivity	σ_L	7.8×10^3	$\Omega^{-1}\,cm^{-1}$	[13]
Solid electrical conductivity	σ_S	3.8×10^3	$\Omega^{-1}\,cm^{-1}$	[13]
Peltier coefficient	Π_{SL}	-0.03	V	from [27] (see Section 2.2)
Liquid Thomson coefficient	τ_L	-7.13×10^{-7}	V/K	[13]
Solid Thomson coefficient	τ_S	4.35×10^{-5}	V/K	[13]

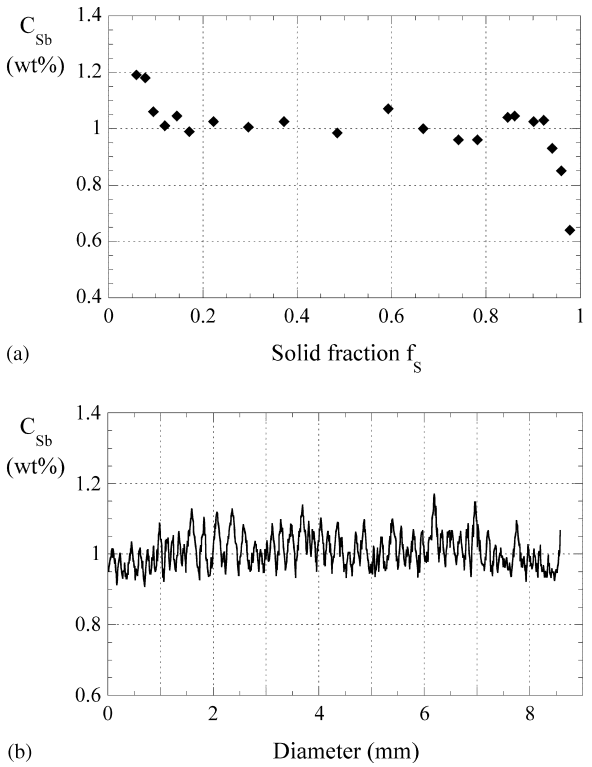

Fig. 2. Longitudinal (a) and radial (b) antimony macrosegregation in solid. $V = 4.17\,\mu m/s$.

terminal transients, the antimony concentration is quite constant along the grown sample which indicates that, if any, bulk convection in the melt during solidification is quite negligible. Moreover, Fig. 2b shows no sign of radial segregation, and thus of fluid flow confined to the vicinity of the S–L interface, the saw-toothed oscillations being due to the partially faceted cellular microstructures which are present for this solidification velocity. Consequently, we can safely consider that the transport is diffusive and the antimony weight fraction in the solid at the interface is equal to the initial alloy content, $C_\phi = 1$ wt%, during steady-state growth. This result is in agreement with Jamgotchian et al. [25], who measured the solute profile in the solid and liquid ahead of the solidification front and concluded that the heat and mass transport was essentially diffusive during directional solidification of Bi–0.5 wt% Sb.

2.2. Solute microsegregation and front velocity induced by PID

For alloys, the very basis of PID technique is the sharp change in solid composition due to the modification of the solute concentration in the liquid at the interface by an electric pulse, which is in contradistinction with pure substances for which the

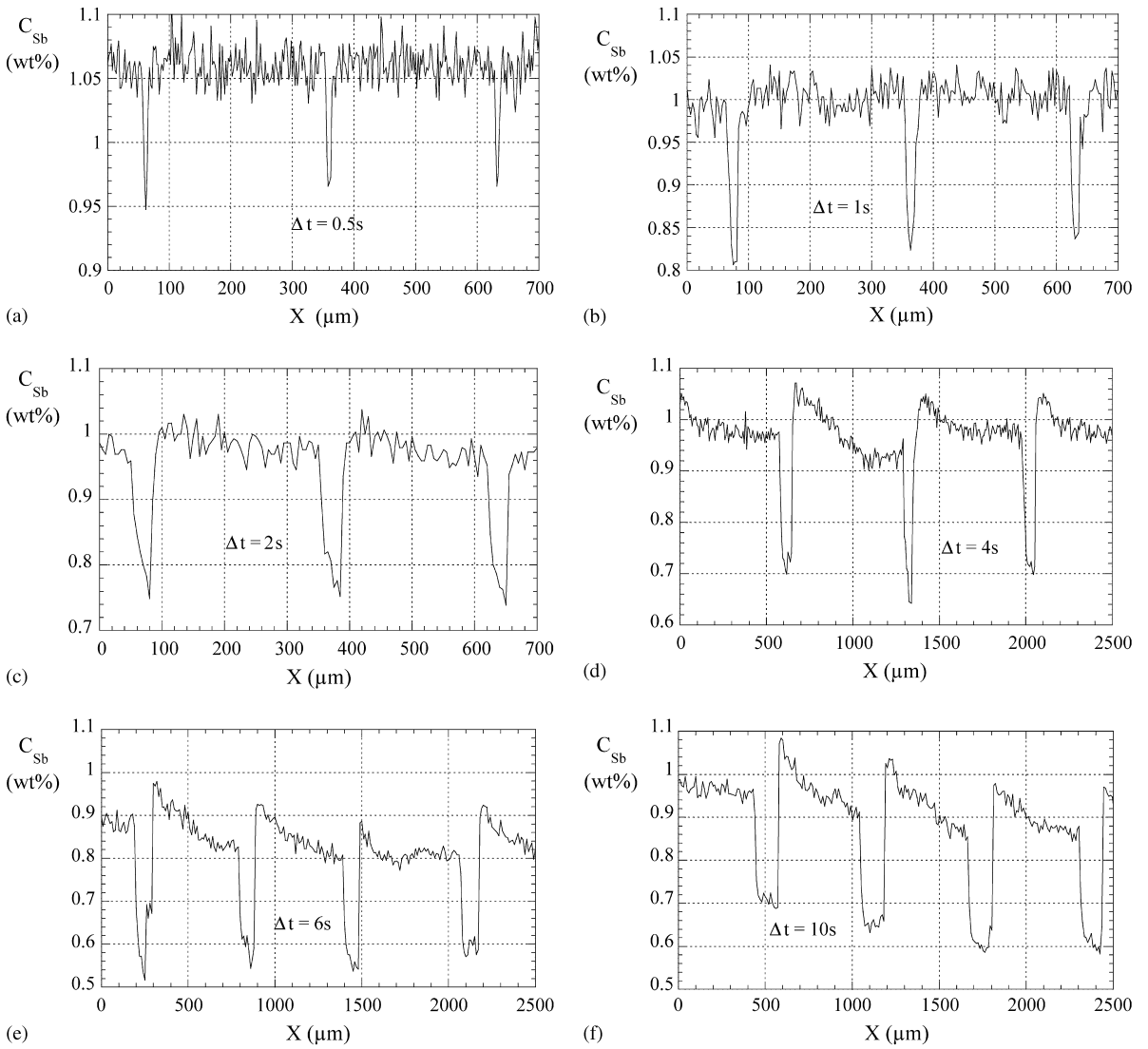

Fig. 3. Electron-probe analysis of antimony microsegregation induced in solid by PID for several pulse durations Δt (a) 0.5 s, (b) 1 s, (c) 2 s, (d) 4 s, (e) 6 s and (f) 10 s.

variation of the S–L interface temperature has to be deduced from measurements with fixed thermocouples [26]. Consequently, measurements of the solute concentration along samples are carried out, for a planar front and through several pulse markings. The solute variation is measured with an electron microprobe for experiments with identical growth conditions ($G = 50\,\mathrm{K/cm}$, $V = 4.17\,\mu\mathrm{m/s}$) and PID parameters ($I = 60\,\mathrm{A/cm^2}$, current direction from solid to liquid) except the pulse duration Δt, that is varied from 0.25 to 10 s.

For each pulse, the series of profiles in Fig. 3 clearly show a sharp decrease in the antimony concentration, down to a minimum value. It should be stressed that a jump is *never* observed at the inception of these peaks. The end of each pulse is

marked by a rapid increase of the solute concentration that ultimately gently goes back to its steady-state value. It is worth noticing that as Δt is increased some overshoot in antimony concentration develops in the transient following the end of each electric pulse. The two steep variations of antimony concentration associated to the switching on and switching off of the electric current have to be related to the two lines that bound each striation when the current direction is from solid to liquid (Fig. 1b). The first one, which appears white in the photograph, corresponds to the pulse initiation at which, due to Peltier cooling, an abrupt but continuous (i.e. *not step-like*) enhancement of interface velocity occurs that results in a decrease of Sb concentration in the adjacent liquid (partition coefficient $k>1$). The second line, which is dark in the picture, comes from the sharp decrease of interface growth velocity at the end of the pulse.

The measurement of the distance between these two lines (Fig. 4a) allows one to estimate the *average* additional velocity ΔV of the S–L interface due to the thermoelectric effects of the electric pulse (Fig. 4b). The line drawn in Fig. 4a suggests that ΔV does not depend on the pulse duration until Δt becomes large enough for slowing down of growth enhancement by Joule heating counteracting Peltier cooling. Also, Fig. 4 already provides the first indication that great care should be taken when, as it has been repeatedly done, the measurement of ΔV and the Peltier coefficient Π_{SL} are directly connected by using the heat balance at the S–L interface

$$L(V+\Delta V)=k_S G_S - k_L G_L - \Pi_{SL} I \tag{3}$$

under the assumption that the temperature gradients in solid and liquid G_S and G_L may be taken as unchanged during the pulses, which gives

$$\Delta V = -\Pi_{SL} I/L. \tag{4}$$

Eq. (4) gives $\Delta V = 34\,\mu m/s$ for $\Pi_{SL} = -0.03\,V$, that is the value calculated for pure Bi from the Kelvin law

$$\Pi_{SL} = T_M(S_S - S_L) \tag{5}$$

and measurements of the Seebeck coefficients in liquid and solid, $S_L \approx 0$ and $S_S = -0.53\times 10^{-5}\,V/K$, respectively [27]. The corresponding

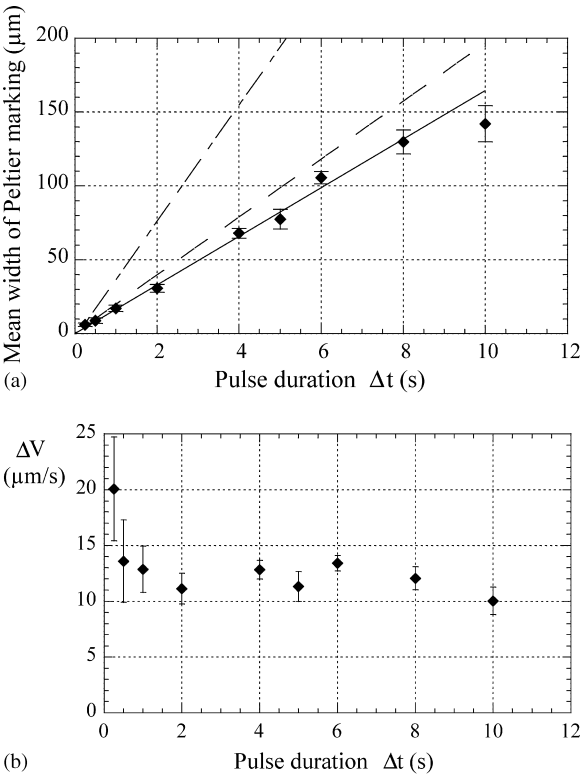

Fig. 4. Variation with pulse duration Δt of (a) mean width of PID striations and (b) mean additional velocity ΔV induced by electric pulse. Dashed line in (a) corresponds to numerical simulation using Brush et al.'s model with Bi kinetics (Eq. (7)), and dot–dashed line to striation width $= 38.17\Delta t$ (see Section 2.2).

striation widths ($= 38.17\Delta t$), plotted in Fig. 4a, are much larger than in experiments, that shows that the usual approach of PID should suffer some deficiency.

3. Comparison with theory

The experimental results presented in Section 2 are now compared with numerical simulations based on the model developed by Brush et al. [10] for the directional solidification of a planar S–L interface in the presence of a time-dependent electric current, using the values in Table 1 for the thermophysical properties of bismuth–antimony alloys.

3.1. Predictions under the assumption of thermodynamic equilibrium at the S–L interface

This case readily corresponds to Brush et al.'s model which assumes that the attachment of atoms at the growth front is infinitely rapid. Fig. 5a shows the variation of interface velocity with the corresponding Sb microsegregation left in solid by an electric pulse given in Fig. 5b. Our data on solute microsegregation *in the pulse* complement previous studies of PID on bismuth, that analysed the variation of the rate of the S–L interface [6,8]. Therefore, in this section, two values are considered for the Peltier coefficient, $\Pi_{SL} = -0.03$ V, i.e. the value in Table 1, and $\Pi_{SL} = -0.014$ V. Indeed, for the sake of consistency the latter value should be rather used when growth kinetics is assumed infinitely fast as it is the one obtained from the fit of Eq. (4) to the magnitude ΔV of the initial velocity jump in experiments on pure Bi, using the Peltier coefficient as an adjustable parameter (see, e.g., Ref. [8]).

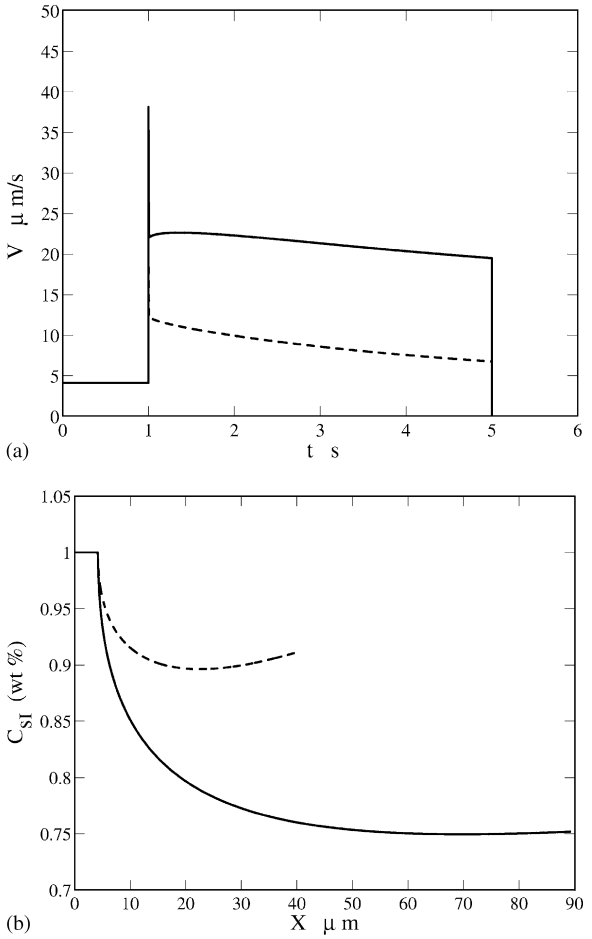

Fig. 5. Numerical simulation with infinitely fast growth kinetics ($\Delta T_k = 0$ in Eqs. 2a and 2b) of (a) growth velocity $V + \Delta V$ and (b) antimony microsegregation induced in solid by PID. $\Delta T = 4$ s. Simulation is stopped when electric current is switched off as backmelting then occurs. Full lines: $\Pi_{SL} = -0.03$ V — Dashed lines: $\Pi_{SL} = -0.014$ V.

In Fig. 5a, a jump in velocity is predicted as the current is switched on. This jump is followed by a very fast transient, that together make a peak, after which the S–L interface velocity slowly decreases. For the current density used in the experiments, $I = 60\ \mathrm{A/cm^2}$, calculations can be only completed until the electric pulse is turned off, because at that time a velocity jump of $-\Pi_{SL}\, I/L$ is predicted to occur that, even for short pulses, induces melting. Besides, the model intrinsically becomes no longer applicable as solute diffusion in the solid is not taken into account. For $\Pi_{SL} = -0.014$ V, during a 4 s-pulse the average growth enhancement, $\Delta V = 5$ μm/s is less than half of what is measured in experiment, $\Delta V = 13$ μm/s (see Fig. 4b), as well as the amplitude of Sb microsegregation left in solid, -0.11 wt% in Fig. 5b compared to -0.28 wt% in Fig. 3d. For $\Pi_{SL} = -0.03$ V, the average growth enhancement $\Delta V = 17$ μm/s, which is now only 30% more than the experimental value, and the amplitude of Sb microsegregation in the pulse, -0.25 wt%, is close to that given by electron microprobe analysis. Yet, it is worth to realise that, in former studies, the physically meaningful value, $\Pi_{SL} = -0.03$ V, would lead to a disagreement by a factor of about 2 for the steep increase in interface velocity at pulse application, to which we have no access in experiment.

A double conclusion follows from this comparison. First, the calculations without kinetics seem very spurious at short times, when the very rapid velocity transient just after the pulse is initiated trying to compensate the instantaneous Peltier cooling ($-\Pi_{SL} I$) by latent heat release ($L\Delta V$), and the neglect of solute diffusion in solid can be of no help as solidification alone takes place. Second, the prediction of Sb microsegregation is good when the

right Peltier coefficient is used, which suggests that, at least for dilute Bi–Sb alloys, the influence of growth kinetics might not be critical all over the electric pulse.

3.2. PID under limited interface kinetics

In order to know the total variation of the S–L interface temperature induced by pulsing (Eqs. 2a and 2b), the relationship between the kinetic undercooling ΔT_k and the growth velocity V is needed. From measurements of Seebeck voltage E_S, Sixou et al. [28] obtained a kinetic law of exponential type in the case of pure bismuth grown without seeding, and concluded that Bi grows by two-dimensional nucleation and lateral spreading of steps. The Seebeck voltage E_S and kinetic undercooling ΔT_k are linked by

$$\Delta T_k = E_S/(S_S - S_L) \tag{6}$$

so that the kinetic law can be obtained from the data in Fig. 4 of Ref. [28]. For tractability in the numerical code, the exponential kinetics is in the following approximated by the power law (Fig. 6):

$$V = 68.1(\Delta T_k)^{4.38} \tag{7}$$

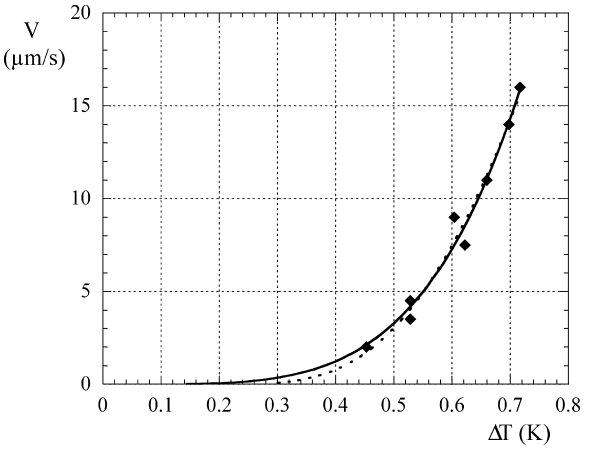

Fig. 6. Variation for bismuth of growth velocity with interface undercooling. Undercooling is deduced from the measurement of Seebeck voltage by Sixou et al. [28]. The fits correspond to the power law approximation Eq. (7) (full line) and the exponential law (dotted line).

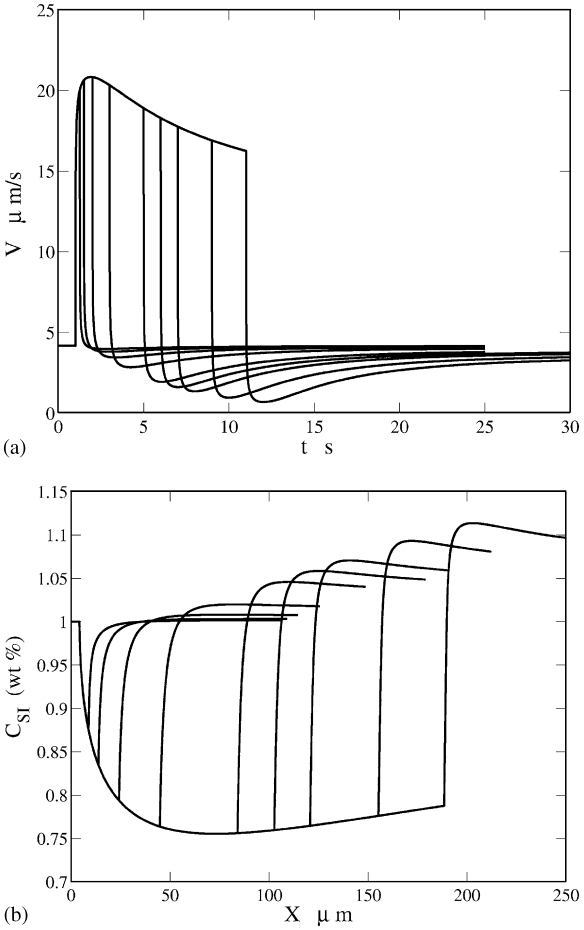

Fig. 7. Numerical simulation with real bismuth kinetics (ΔT_k given by Eq. (7)) of (a) growth velocity $V + \Delta V$ and (b) antimony microsegregation induced in solid by PID. $\Delta t = 0.25, 0.5, 1, 2, 4, 5, 6, 8$ and 10 s.

with V in μm/s and ΔT_k in K. It follows from Fig. 6 that the difference between this power law and the exponential law is very much negligible for interface velocities above the pulling rate (4.17 μm/s), i.e. in the active part of PID by Sb segregation (see e.g. Fig. 7). Besides, the difference near $V = 0$ remains slight.

For a binary alloy, a possible experimental way to get ΔT_k is to directly measure the value of interface temperature T_ϕ and concentration C_ϕ as a function of interface velocity V. By using Eq. (1),

one would then be able to deduce ΔT_k as a function of V. Using a directional solidification set-up, one might think of using the measurements of the S–L interface temperature during melting and solidification at the same velocity. Such an attempt is bound to fail due to the strong asymmetry between melting, in which the interface is largely rough, and freezing, in which kinetic undercooling is several orders of magnitude larger at low growth rates, as evidenced for instance by Honeyman and Small for a faceting material, salol, and a non-faceting one, carbon tetrabromide [29].

Numerical simulations for Bi–1 wt% Sb using the Brush et al.'s model [10] with the boundary condition giving interface temperature modified to include Eq. (7) for finite kinetics are shown in Fig. 7. Now, instead of jumping by the quantity $-\Pi_{SL} I/L$ ($= 34\,\mu m/s$) when electric current is switched on, the interface velocity rather rapidly increases only to values of about $20\,\mu m/s$ (Fig. 7a), which means that Peltier cooling is never totally transformed into additional solidification. For pulses longer than 1 s the growth rate goes through a maximum after which it slowly decreases due to Joule heating. Moreover, sluggish kinetics of bismuth suppresses backmelting when the current is switched off so that it becomes possible to compute antimony segregation in solid before, during and *after* the electric pulse (Fig. 7b). Microsegregation amplitude increases with pulse duration Δt till a maximum a little before 4 s. After the pulse, Sb concentration returns to its steady-state value with an overshoot. After normalisation of the baselines in Fig. 3 to $C_{SI} = 1$ wt%, the evolution in experiments of the value $C_{SI,m}$ at maximum Sb segregation in the pulses, and of the value $C_{SI,M}$ at maximum overshoot shows quantitative agreement with numerical results (Fig. 8), a small difference being certainly within the error bar due to the uncertainties in the thermophysical coefficients. This agreement is not fortuitous but reliable because simulations are carried out on sound bases: (i) the values of the thermoelectric coefficients of bismuth given in Table 1 are coherent as obtained in the same group [13], as well as the kinetic law (Eq. (7)), (ii) all parameters in the theoretical model are known so that there is no degree of freedom for adjustment. Furthermore, the theoretical width of markings also agrees well with experiment (see Fig. 4a). Therefore, Brush et al.'s model with kinetics can be taken as predictive, its precision being in practice mostly linked to that of thermoelectric coefficients and kinetic relationship.

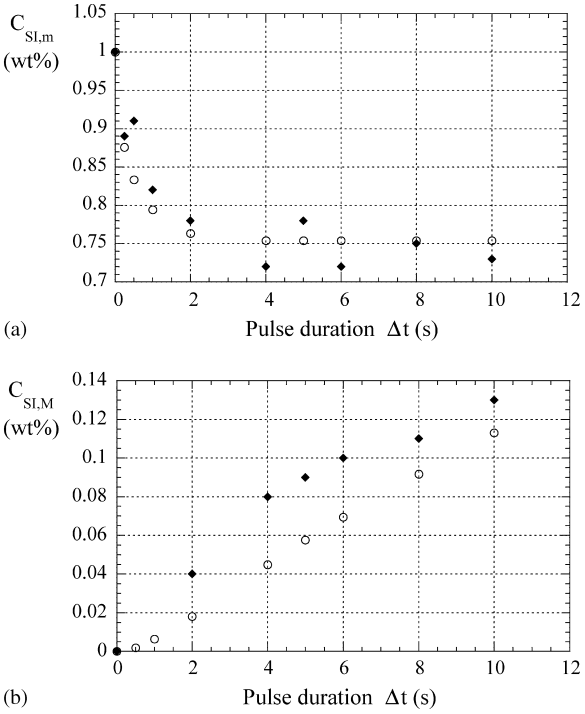

Fig. 8. Variation with pulse duration Δt of antimony concentration at: (a) maximum segregation in the pulse, $C_{SI,m}$, and (b) at maximum overshoot, $C_{SI,M}$. (◆): experiment, (○): numerical simulation.

From the kinetic law given by Eq. (7) and Fig. 7, values of 0.23 and 0.22 K are obtained for the interface undercooling ΔT_k due to growth kinetics, for the interface velocities at the end of the 0.25 and 4 s-pulses, respectively, that is of the same order of magnitude than the values, 0.42 and 0.85 K, of the concomitant solutal undercoolings ΔT_C ($= -n[(C_S)_t - (C_S)_0]$). Besides, for very short pulses ΔT_k even gives the dominant contribution to the change in S–L interface temperature (e.g. $\Delta T_k = 0.143$ K against $\Delta T_C = 0.025$ K for a 0.01 s-pulse). Therefore, the conclusion forces itself that one should abandon the hypothesis of local equilibrium at the S–L interface during an electric pulse and take into

account kinetics in the analysis of PID, the shorter the electric pulse the more mandatory the requirement. Moreover, for the Bi–Sb thermophysical properties in Table 1, a kinetic law different from Eq. (7) may have a pronounced effect on solute microsegregation in PID and thus actually dominate marking characteristics for somewhat long pulses as illustrated in Fig. 9 using a quadratic law $V = \mu(\Delta T_k)^2$ with different values of μ, which indicates that the agreement obtained in Section 3.1 without kinetics is very likely not a general feature of PID.

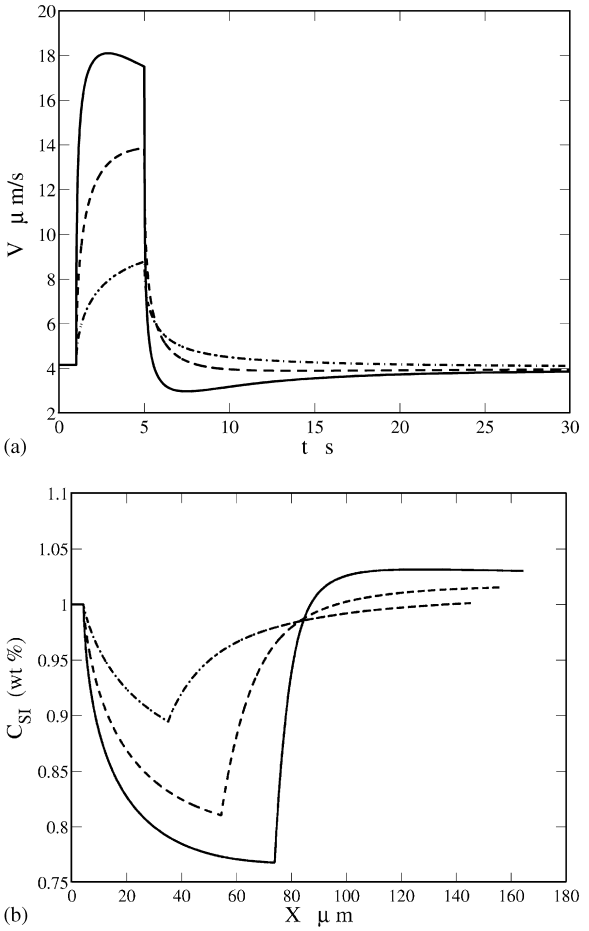

Fig. 9. Numerical simulation with kinetics rendered more sluggish than in bismuth by using the quadratic law $V = \mu(\Delta T_k)^2$. (a) Growth velocity $V + \Delta V$. (b) Antimony microsegregation induced in solid by PID. $\Delta t = 4$ s. Kinetic coefficient $\mu = 0.1$, 1 and 10 μ/s K^2 (dot–dashed, dashed and solid curves, respectively).

For practical application, a compromise has to be achieved. Indeed, there should be enough Sb segregation for clear metallography, suggesting the use of long pulses, together with thin striations giving sharp outline of the interface morphology, that instead suggests the application of short pulses. Fig. 7b confirms the conclusion drawn in previous experimental analysis of PID on Bi–1 wt% Sb, namely that $\Delta t = 0.5$ s is the good choice [12].

From the present study of PID on Bi–1 wt% Sb alloys, two conditions can be proposed to select systems which are prone to efficient PID. First, high Peltier coefficient Π_{SL} is a necessary condition, which is well illustrated by the fact that PID has up to now been reserved to semimetals and semiconductors. Second, a flat solidus is very much favourable for sharp and visible interface marking by PID striations, as a small change in interface temperature then induces a large variation in solute concentration in solid.

3.3. Inception of interface demarcation in electric pulse

For the solute field, as Fig. 7 shows that solidification front velocity and Sb concentration in solid are both continuous in the pulse, it directly results from the interfacial solute balance that, in the absence of electromigration, the solute gradient at the interface in the liquid is also continuous at the switching on of electric current, as well as interface temperature T_ϕ from Eqs. 2a and 2b.

Therefore, the main effect of the pulse application is felt through the heat balance boundary condition, which reads

$$k_S G_S - k_L G_L = LV \quad \text{at } t \to 0^-, \tag{8a}$$

$$k_S(G_S + \Delta G_S) - k_L(G_L + \Delta G_L) = LV + \Pi_{SL} I \quad \text{at } t \to 0^+, \tag{8b}$$

so that

$$k_S \Delta G_S - k_L \Delta G_L = \Pi_{SL} I \quad \text{at } t \to 0^+. \tag{8c}$$

The compensation in Eq. (8c) of Peltier cooling by the modification of G_S and G_L corresponds to the

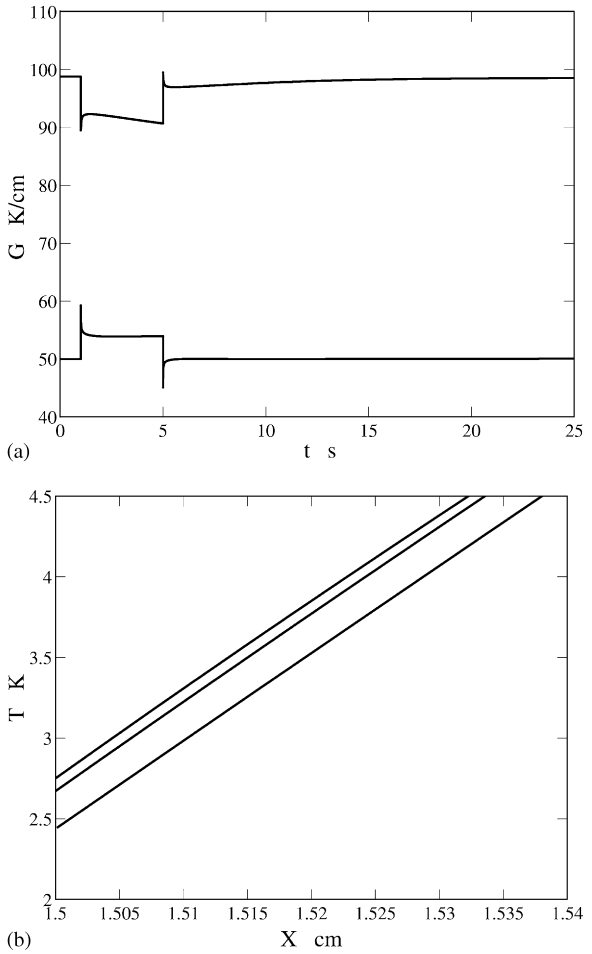

Fig. 10. Numerical simulation of (a) the evolution of the thermal gradients, G_S in solid (upper curve) and G_L in liquid (lower curve), and (b) the temperature profile in the melt: $t = 0.01$ s (upper curve), 0.02 s (middle), 0.1 s (lower). $X = 1.50$ corresponds to the position of the S–L interface; the temperature scale is relative to the melting point of pure bismuth so that for steady state growth at $V = 4.17\,\mu$m/s the interface temperature is 3.45 K for infinite kinetics and 2.92 for Bi kinetics (Eq. (7)).

first peaks in Fig. 10a that shows the evolution of the temperature gradients in melt and solid. This scenario is rigorously proved by the detailed theoretical analysis of the first moments of PID by means of Laplace transform presented in a companion paper [30]. It is worth noting that, at the S–L interface, G_S and G_L then relax within a fraction of a second, actually in less than a tenth of a second (Fig. 10b), due to very fast transfer of a major part of Peltier cooling into enhancement of growth rate.

The major consequence of this analysis, that should be strongly emphasised, is that the usual assumption that the temperature gradients at the crystal–melt interface may be taken as unchanged during a pulse sequence, in which case from Eq. (8b) there is an instantaneous jump in growth rate to absorb Peltier cooling, is not valid. Actually, as finite attachment kinetics introduces inertia that impedes velocity jump it is just the opposite that holds when electric current is applied: *only* thermal gradients are effected at pulse inception, and all other fields and gradients, and growth velocity, are continuous, and adjust subsequently.

4. Conclusion

By a joint approach combining detailed experimental analysis of solute microsegregation and numerical simulation, the fundamental mechanisms acting in PID during directional solidification of Bi–1 wt% Sb alloy are evidenced. It is proved that the usual assumption of thermodynamic equilibrium at the S–L can no longer be sustained, and that it is mandatory to incorporate finite kinetics in theoretical modelling. For short pulses, this constraint is likely to be strong in practical application of PID as the kinetic law should be *appropriate* to the system under study, in particular because attachment kinetics is generally not linear for systems with high Peltier coefficient.

Consequently, it remains conceivable to use thermoelectric effects, and thus PID, and fitting of numerical simulation to determine atomic kinetics of solidification, as proposed by Schaefer and Glicksman [31], which nevertheless presupposes that all thermophysical coefficients are known with good precision, especially the Peltier coefficient Π_{SL} that can be obtained from the measurement of thermoelectric power.

Acknowledgements

The financial support from the Centre National d'Etudes Spatiales (CNES), that made this work

possible, is gratefully acknowledged, as is also the support from the Microgravity Research Division of NASA. The authors wish to thank Mrs. F. Robaut (Consortium des Moyens Technologiques Communs, Grenoble) for the microprobe measurements.

References

[1] W.W. Mullins, R.F. Sekerka, J. Appl. Phys. 35 (1964) 444.
[2] J.A. Warren, J.S. Langer, Phys. Rev. E 47 (1993) 2702.
[3] B. Caroli, C. Caroli, L. Ramirez-Piscina, J. Crystal Growth 132 (1993) 377.
[4] W. Huang, Q. Wei, Y. Zhou, J. Crystal Growth 100 (1990) 26.
[5] W.J. Boettinger, J.A. Warren, Met. Trans. A 27 (1996) 657.
[6] W.G. Pfann, K.E. Benson, J.H. Wernick, J. Electron. 2 (1957) 597.
[7] W.G. Pfann, R.S. Wagner, Trans. Met. Soc. AIME 224 (1962) 1139.
[8] J.M. Bardeen, B.S. Chandrasekhar, J. Appl. Phys. 29 (1958) 1372.
[9] M.J. Wargo, A.F. Witt, J. Crystal Growth 66 (1984) 541.
[10] L.N. Brush, S.R. Coriell, G.B. McFadden, J. Crystal Growth 102 (1990) 725.
[11] L.L. Zheng, D.J. Larson, J. Crystal Growth 180 (1997) 293.
[12] Q. Li, H. Nguyen Thi, B. Billia, J. Crystal Growth 167 (1996) 277.
[13] S. Corre, T. Duffar, M. Bernard, M. Espezel, J. Crystal Growth 180 (1997) 604.
[14] A.F. Witt, M. Lichtensteiger, H.C. Gatos, J. Electrochem. Soc. 120 (1973) 1119.
[15] A.F. Witt, M. Lichtensteiger, H.C. Gatos, J. Electrochem. Soc. 121 (1974) 787.
[16] A. Murgai, H.C. Gatos, W.A. Westdorp, J. Electrochem. Soc. 126 (1979) 2240.
[17] A.F. Witt, H.C. Gatos, J. Electrochem. Soc. 114 (1967) 413.
[18] D.E. Holmes, H.C. Gatos, J. Appl. Phys. 52 (1981) 2971.
[19] A.A. Wheeler, S.R. Coriell, G.B. McFadden, J. Crystal Growth 88 (1988) 1.
[20] S.R. Coriell, G.B. McFadden, A.A. Wheeler, D.T.J. Hurle, J. Crystal Growth 94 (1989) 334.
[21] A.A. Wheeler, S.R. Coriell, G.B. McFadden, D.T.J. Hurle, J. Crystal Growth 100 (1990) 78.
[22] M. Adda Bedia, M. Ben Amar, Phys. Rev. E 51 (1995) 1268.
[23] A.J. Goss, in: J.J. Gilman (Ed.), The Art and Science of Growing Crystals, Wiley, New York, 1963, p. 314.
[24] W.M. Yim, J.P. Dismukes, in: H.S. Peiser (Ed.), Crystal Growth, Pergamon Press, Oxford, 1967, p. 187.
[25] H. Jamgotchian, B. Billia, L. Capella, J. Crystal Growth 62 (1983) 539.
[26] R.P. Silberstein, D.J. Larson, Mat. Res. Soc. Symp. Proc. 87 (1987) 129.
[27] J.J. Favier, DSc Thesis, INPG, Grenoble, France, 1977.
[28] B. Sixou, A. Rouzaud, J.J. Favier, J. Crystal Growth 137 (1994) 605.
[29] W.N. Honeyman, M.B. Small, J. Crystal Growth 21 (1974) 155.
[30] S.R. Coriell, G.B. McFadden, B. Billia, H. Nguyen Thi, Y. Dabo, J. Crystal Growth 216 (2000) 495.
[31] R.J. Schaefer, M.E. Glicksman, Acta Met. 16 (1968) 1009.